




# Effect of space flight on the behavior of human retinal pigment epithelial ARPE-19 cells and evaluation of coenzyme Q10 treatment

Francesca Cialdai<sup>1</sup> · Davide Bolognini<sup>2</sup> · Leonardo Vignali<sup>1</sup> · Nicola Iannotti<sup>3</sup> · Stefano Cacchione<sup>4</sup> · Alberto Magi<sup>5</sup> · Michele Balsamo<sup>6</sup> · Marco Vukich<sup>6</sup> · Gianluca Neri<sup>6</sup> · Alessandro Donati<sup>6</sup> · Monica Monici<sup>1</sup> · Sergio Capaccioli<sup>7</sup> · Matteo Lulli<sup>7</sup> 

Received: 30 June 2021 / Revised: 20 September 2021 / Accepted: 13 October 2021 / Published online: 29 October 2021  
© The Author(s), under exclusive licence to Springer Nature Switzerland AG 2021

## Abstract

Astronauts on board the International Space Station (ISS) are exposed to the damaging effects of microgravity and cosmic radiation. One of the most critical and sensitive districts of an organism is the eye, particularly the retina, and > 50% of astronauts develop a complex of alterations designated as spaceflight-associated neuro-ocular syndrome. However, the pathogenesis of this condition is not clearly understood. In the current study, we aimed to explore the cellular and molecular effects induced in the human retinal pigment ARPE-19 cell line by their transfer to and 3-day stay on board the ISS in the context of an experiment funded by the Agenzia Spaziale Italiana. Treatment of cells on board the ISS with the well-known bioenergetic, antioxidant, and antiapoptotic coenzyme Q10 was also evaluated. In the ground control experiment, the cells were exposed to the same conditions as on the ISS, with the exception of microgravity and radiation. The transfer of ARPE-19 retinal cells to the ISS and their living on board for 3 days did not affect cell viability or apoptosis but induced cytoskeleton remodeling consisting of vimentin redistribution from the cellular boundaries to the perinuclear area, underlining the collapse of the network of intermediate vimentin filaments under unloading conditions. The morphological changes endured by ARPE-19 cells grown on board the ISS were associated with changes in the transcriptomic profile related to the cellular response to the space environment and were consistent with cell dysfunction adaptations. In addition, the results obtained from ARPE-19 cells treated with coenzyme Q10 indicated its potential to increase cell resistance to damage.

**Keywords** Retina · Microgravity · Radiation · Retinopathy · Space flight

## Introduction

Space radiation and microgravity present in spacecraft and space stations in orbit around the Earth cause several time-dependent health alterations in astronauts both during

their missions and after their return to Earth. The most well-known are fluid shifts, loss of bone and muscle mass, cardiovascular imbalances, alterations in immunity, sleep interruption, and circadian misalignment, which have been described for more than two decades in a multitude of scientific reports and reviews [1–6]. At the cellular level, the main pathological effects of microgravity and cosmic radiation

---

Sergio Capaccioli and Matteo Lulli contributed equally to this study.

---

✉ Matteo Lulli  
matteo.lulli@unifi.it

<sup>1</sup> ASAcampus Joint Laboratory, ASA Res. Div., Department of Experimental and Clinical Biomedical Sciences “Mario Serio”, Università Degli Studi Di Firenze, Firenze, Italy

<sup>2</sup> Department of Experimental and Clinical Medicine, Università Degli Studi Di Firenze, Firenze, Italy

<sup>3</sup> Department of Life Sciences, Università Degli Studi Di Siena, Siena, Italy

<sup>4</sup> Department of Biology and Biotechnology “Charles Darwin”, Università Di Roma “La Sapienza”, Roma, Italy

<sup>5</sup> Department of Information Engineering, Università Degli Studi Di Firenze, Firenze, Italy

<sup>6</sup> Kayser Italia S.R.L., Livorno, Italy

<sup>7</sup> Department of Experimental and Clinical Biomedical Sciences “Mario Serio”, Università Degli Studi Di Firenze, viale Morgagni 50, 50134 Firenze, Italy

are structural alterations caused by free radical-mediated molecular damage [7–10].

Space exploration has now entered a new phase in which NASA, ESA, and other national space agencies are working together to plan long-term space missions in order, for example, to create lunar bases and reach other space destinations such as Mars. At this stage, assessing the risk inherent in space missions and challenging the numerous obstacles to astronaut safety are increasingly important in mission planning. In particular, since the microgravity and ionizing radiation inevitably present in the spacecraft environment represent two serious stress factors for astronaut health, the discovery of pharmacological countermeasures is clearly a mandatory prerequisite for mission planning [11, 12]. A basic principle of pharmacological research is that the most valid rational basis for identifying tools capable of blocking or inhibiting a pathological process is knowledge of its pathogenic mechanisms. This principle applies to the range of damage and health impairments known to be endured by astronauts during their lengthy space missions.

The eye, particularly the retina, is severely sensitive to radiation and microgravity damage, which eventually cause apoptotic cell death [9, 10, 13–18]. Approximately 10 years ago, NASA reported that nearly 60% of 300 astronauts returning to Earth after long-term stay aboard the International Space Station (ISS) were affected by several neurophthalmic alterations, including optic disc edema, globe flattening, choroidal and retinal folds, hyperopic refractive error shifts, nerve fiber layer infarcts, and visual acuity reduction [19], comprehensively termed spaceflight associated neuro-ocular syndrome (SANS) [20–23]. The pathogenesis of SANS is not fully understood. The relevance of astronauts' visual impairment led NASA to consider vision as one of the top health risks for long-term space flight [24].

The ISS, where astronauts are exposed to the space environment for several months [25], offers a great opportunity to directly study astronaut health impairments, but also to execute experiments aimed at unraveling the pathogenesis of damage even at the molecular level and to test the efficacy of potential countermeasures to minimize damage and therefore maximize the feasibility of space missions.

In this paper, we aimed to explore the impact exerted on both the cell structure and on the transcriptomic profile by the transfer of human retinal pigment epithelial ARPE-19 cells from the Earth to the ISS and their subsequent culture on board for 3 days. The effects of coenzyme Q10 (CoQ10) treatment, by virtue of its well-known antioxidant and anti-apoptotic abilities [26–29], are also reported. The results presented here were obtained in the context of the project “The Coenzyme Q10 (CoQ10) as Countermeasure for Retinal Damage on board the International Space Station: the CORM Project”, funded by the Agenzia Spaziale Italiana (ASI) and belonging to a group of investigations of the ESA

VITA (*Vitality, Innovation, Technology, Ability*) mission, which have been included in the ISS expedition 52/53. To optimize the conditions for the experiment aboard the ISS, we previously carried out on-ground experiments revealing that a 3-day stay in simulated microgravity (using a rotating wall vessel bioreactor) led ARPE-19 cells to undergo apoptosis, while X-rays induced a dose-dependent DNA damage accompanied by a DNA damage response at telomeres, referred to as telomere dysfunction-induced foci accumulation [26].

## Material and methods

### Cell culture

Human retinal pigment epithelial ARPE-19 cells (ATCC, Manassas, VA, USA) were cultured in 50% Dulbecco's modified Eagle's medium (DMEM, Lonza, Basel, CH) and 50% Ham's F12 Medium (Lonza) supplemented with 10% fetal bovine serum (FBS; # 35–015-CV; Corning, NY, USA), 100 U/mL penicillin–streptomycin (Lonza), and 2 mM L-glutamine (Lonza) in a humidified incubator at 37 °C and 5% CO<sub>2</sub>. ARPE-19 cells were frozen and shipped to the Kennedy Space Center (KSC) Space Station Processing Facility (SSPF) laboratories (Cape Canaveral, Florida, USA) months before the scheduled launch date. Two weeks before launch, the cells were thawed and cultured in the KSC laboratories. For the experiment on board the ISS, ARPE-19 cells were seeded at a density of 20,000 cells/cm<sup>2</sup> on cell culture supports, i.e., cyclic olefin copolymer (COC) ibiTreat plastic coverslips (IBIDI, Martinsried, Germany), which allow cell adhesion that is comparable to standard cell culture flasks, flexibility, and good optical performance. Dedicated experimental units (EUs, KEU-ST, Kayser Italia, Livorno, Italy), which are electromechanical devices capable of executing cell culture protocols and are qualified for flights to the ISS, were used for the experiment on board the ISS (Fig. 1A–B). EUs contain five reservoirs: three were loaded with cell culture media (50% DMEM, 50% Ham's F12, 10% FBS, 100 U/mL Penicillin–Streptomycin, 2 mM L-Glutamine, 25 mM Hepes [Lonza]) in the presence or absence of 10 μM CoQ10 (Sigma-Aldrich, St. Louis, USA) dissolved in a commercial vehicle to ensure cellular uptake (0.04% Kolliphor P407 micro, Sigma-Aldrich); one with Dulbecco's phosphate-buffered saline (DPBS, added with Ca<sup>2+</sup>/Mg<sup>2+</sup>, Lonza) for cell rinse prior to fixation; one with RNAlater (Ambion AM7020, MA, USA) as a fixative solution. At day 1 after seeding, cell cultures on COC plastic coverslips were transferred into the cell culture chambers of the EUs, which were then introduced into Experiment Containers KIC-SL to compose the experimental hardware (EH). EUs were inserted into a passive temperature-controlled transportation

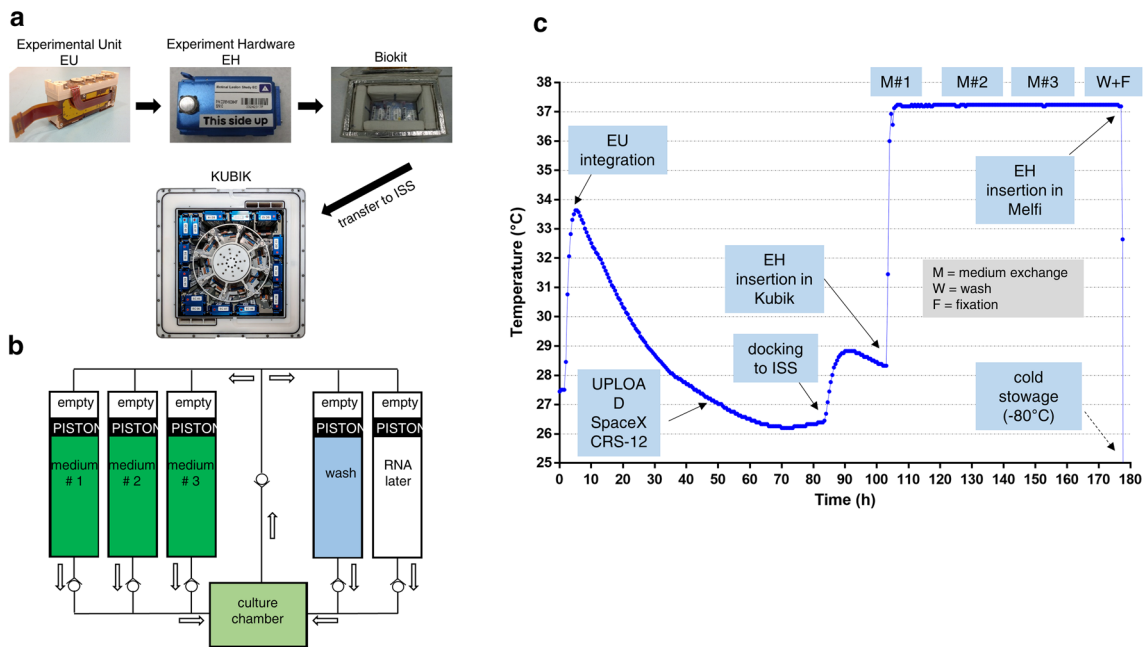


**Fig. 1** **A** The hardware of CORM experiment: the experimental units (EUs) were integrated into experimental containers to compose the experiment hardware (EH), which were placed inside the Biokit transportation container that was launched to the International Space

Station (ISS). Once onboard ISS, the EH were inserted into the ESA KUBIK incubator in the ISS Columbus module. **B** Schematic fluidic of the EU. **C** iButton data logger-derived temperature profile of the CORM experiment

container, named Biokit (Kayser Italia), containing phase-change materials preheated at 27 °C. An iButton data logger was placed on an EH to record the temperature every minute until the end of the experiment (the recorded temperature profile is shown in Fig. 1C). Three EHs were transferred to flight authorities (two containing cells not treated with CoQ10, and one containing cells treated with CoQ10) on day 2 after cell seeding. On August 14, 2017, the hardware was launched on a Dragon/Falcon 9 vector in the framework of the Space X CRS-12 mission on day 3 after seeding; it reached the ISS on day 5. On board the ISS, astronaut Paolo Nespoli manually inserted the EHs into the ESA KUBIK incubator set at 37 °C to power the EHs. Fluidic activations were automatically performed, allowing media replacement on days 6, 7, and 8 after seeding, and rinsing and fixation on day 9. In particular, fixation with RNAlater occurred 5 min after rinsing with DPBS saline solution. In total, the EHs spent 72 h inside the KUBIK facility. The samples were then manually transferred into the Minus Eighty Laboratory Freezer for ISS (MELFI) refrigerator by astronaut Paolo Nespoli and stored at -80 °C until their return to Earth on September 16, 2017. The temperature profile was downloaded from the data logger, allowing the reproduction of the same time/temperature profile as that of the ground control experiments. Once on the ground, the samples were thawed and retrieved from the EUs. COC plastic coverslips containing cells were sectioned with a scalpel while they were

continuously submerged in RNAlater. Five sections were obtained from each sample: one was subjected to apoptosis evaluation through TUNEL assay, one to vimentin immunofluorescence analysis, and three to transcriptomic analysis. Images of cells were acquired by optical microscopy using an EVOS XL Core Imaging System (Thermo Fisher Scientific, USA).

## Tunel

The DeadEnd Fluorometric TUNEL System kit (Promega, USA) was used to detect DNA breaks according to the manufacturer's protocol. Briefly, samples were fixed in 4% formaldehyde solution in PBS for 25 min at +4 °C and washed twice with PBS. The cells were then permeabilized with 0.2% Triton X-100 in PBS for 5 min. After washing with PBS, the samples were incubated in equilibration buffer from the staining kit for 10 min and then treated with staining reaction mix for 1 h at 37 °C in a humidified chamber protected from light. The reaction was arrested by incubation for 15 min in 2×SSC. After washing with PBS, cells were stained with Hoechst 33,242 dye (40,6-diamidino-2-phenylindole; Thermo Fisher Scientific) for 10 min and mounted with ProLong Diamond Antifade Mountant (Thermo Fisher Scientific). For a positive staining control, the slides were treated after permeabilization with DNase I (10 units/mL)

for 10 min. The samples were analyzed using a confocal microscope (Nikon TE2000 using EZ-C1 Software; Nikon Corp.) equipped with a 60XA/1.40 oil-immersion objective and digitally captured.

## Immunofluorescence

Cells grown on plastic coverslips and treated as previously described were fixed for 5 min with ice-cold acetone. Unspecific binding sites were blocked with PBS containing 3% bovine serum albumin (BSA; Sigma-Aldrich) for 1 h at  $22 \pm 2$  °C. The cells were then incubated overnight at 4 °C with anti-vimentin antibody (#MAB1681, Chemicon, Merck KGaA, Darmstadt, Germany) diluted 1:100 in PBS with 0.5% BSA. After washing three times with PBS-0.5% BSA, samples were incubated for 1 h at  $22 \pm 2$  °C in the dark with fluorescein isothiocyanate-conjugated secondary antibody (anti-mouse IgM [#AP128F, Chemicon] diluted 1:200). The samples were washed three times, mounted on glass slides using Fluoromount™ aqueous mounting medium (Sigma-Aldrich), evaluated using an epifluorescence microscope (Nikon, Firenze, Italy) at 100× magnification, and imaged using a HiRes IV digital CCD camera (DTA, Pisa, Italy).

## RNA isolation

RNA extraction was performed using the RNAqueous Total RNA Isolation kit (Ambion AM1912) following the manufacturer's instructions, and 40 µL RNA was eluted. The samples were vacuum-concentrated using DNA 120 Speedvac® (ThermoSavant, USA) with low vacuum and no heating to avoid RNA fragmentation, and the samples were manually checked every 5 min until the volume reached 20 µL. Residual genomic DNA was removed using a DNA-free DNA Removal kit (Ambion AM1906) following the manufacturer's instructions. Isolated RNA and library preparation products were quantified using Qubit 3.0 (Invitrogen, USA) and quality was assessed by capillary electrophoresis using an AATI Fragment Analyzer (Advanced Analytical Technologies, Inc., USA).

## Gene expression analysis

RNA expression was quantified at Polo d'Innovazione di Genomica, Genetica e Biologia (Polo GGB, Siena, Italy) using RNAseq analysis. Total ribo-depleted cDNA libraries were prepared using SMARTer Stranded Total RNA-Seq Kit Pico Input Mammalian (Takara Bio USA, Inc.) according to the manufacturer's instructions. Indexed DNA libraries were normalized to a concentration of 4 nM and then pooled in equal volumes to obtain a uniform read distribution. The pool was denatured and diluted to a final loading concentration of 1.4 pM according to the Illumina protocol, with the

addition of 1% spike in PhiX Control v3 (Illumina, USA) as a sequencing control. To obtain a minimum of 20 million reads per sample, the pool was sequenced using a NextSeq 550 sequencer (Illumina) using a NextSeq 500/550 Mid Output v2 kit (150 cycles) (Illumina) to perform a paired-end run 2X75 bp read length.

Raw reads for each sample (three treated vs. three untreated replicates) were aligned to the human\_g1k\_v37 release of the GRCh37/hg19 human reference genome using the RNA-seq aligner STAR [30] (version 2.5.2b) with the default parameter settings. Count-based differential expression analysis was performed using featureCounts [31] and DESeq2 [32]. In detail, we counted the reads mapped to each genomic meta-feature (that is, each gene) with featureCounts (version 1.5.1), using the default parameter settings and the Ensembl Gene Transfer Format (GTF) file for the appropriate reference genome (Ensembl release 82). The count matrix from featureCounts (where each row represents an Ensembl gene, each column is a sequenced RNA library, and the values indicate the raw numbers of fragments that were uniquely assigned to the respective gene in each library) was subsequently converted into a *DESeqDataSet* object inside the R statistical environment. The downstream differential expression analysis in the DESeq2 R package (release 3.3) uses a generalized linear model of the form  $K_{ij} \sim \text{NB}(\mu_{ij}, \alpha_i)$ , where  $K$  counts (from the count matrix) for gene  $i$  and sample  $j$  are modeled using a negative binomial (NB) distribution with mean  $\mu_{ij}$  and gene-specific dispersion  $\alpha_i$ , which defines the relationship between the variance of the observed count and its mean value. The estimation of the dispersion values for each gene as well as the fitting of the NB distribution were performed using the *DESeq* function, and the log fold change (LFC) estimates,  $p$  values, and adjusted  $p$  values (Wald statistic, treated vs. untreated) were extracted using the *results* function using the default parameter settings. To generate even more accurate LFC estimates, we eventually calculated shrunken LFC estimates (*lfcShrink* function, *apeglm* algorithm): LFC shrinkage uses LFC estimates for all genes to shrink toward the LFC estimates of genes with little information (low counts) or high dispersion, facilitating the downstream assessment of results.

## Pathway analysis

The data were analyzed using the iPathwayGuide platform in the context of pathways obtained from the Kyoto Encyclopedia of Genes and Genomes (KEGG) database (Release 84.0 +/10–26, Oct 17), gene ontologies from the Gene Ontology (GO) Consortium database (2017-Nov6), miRNAs from the miRBase (Release 21), and TARGETSCAN (TargetsCan version: Mouse:7.1, Human:7.1) databases. iPathwayGuide scores pathways using the impact analysis method [33], which uses two types of evidence: (i) the

over-representation of differentially expressed (DE) genes in a given pathway and (ii) the perturbation of that pathway computed by propagating the measured expression changes across the pathway topology. These aspects are captured by two independent probability values, pORA and pAcc, which are then combined in a unique pathway-specific  $p$  value. pORA expresses the probability of observing the number of DE genes in a given pathway that is equal to or greater than that observed by random chance. pAcc was calculated based on the amount of total gene accumulation measured in each pathway. Once the accumulations of all gene number perturbations are computed, iPathwayGuide computes the total accumulation of the pathway as the sum of all absolute accumulations of the genes in a given pathway. The two types of evidence, pORA and pAcc, are combined into one final pathway score by calculating a  $p$  value using Fisher's method, which is then rectified for multiple comparisons using false discovery rate (FDR) or Bonferroni correction. Bonferroni correction, which is simpler and more conservative than FDR, reduces the false discovery rate by imposing a stringent threshold on each comparison adjusted for the total number of comparisons. FDR correction has more power, but only controls the family-wise false positive rate.

## Results

As previously described and shown in Fig. 1, the CORM experiment was set up in the NASA KSC SSPF laboratory (Cape Canaveral, Florida, USA), where ARPE-19 cells (treated with CoQ10 or not) were seeded in a dedicated EU, which was then introduced into the EC to compose the EH [26] (Fig. 1A). The EH was included in the passive temperature-controlled transport container Biokit, which was launched to the ISS in the context of SpaceX CRS-12. Three EHs were transferred to the ISS: two containing cells not treated with CoQ10, and one containing cells treated with CoQ10. Biokit's transfer to the ISS lasted 3 days, during which the cells underwent a constant decrease in temperature up to approximately 26 °C. Once on board the ISS, the EHs were moved to the ESA KUBIK (incubator facility), set at 37 °C, allowing the automatic execution of fluidic activations according to the programmed schedule (Fig. 1B). After 3 days, the cells were fixed in RNAlater and the EHs were stored at – 80 °C in the MELFI, where they were kept until splashdown. Once in our laboratories, under freezing conditions, the EH underwent final disassembly, and the samples were inspected. Ground ARPE-19 cell cultures were also prepared as controls under normal gravity using a similar EH, following the temperature/time profile of the in-flight experiment (Fig. 1C).

### Transferring ARPE-19 cells to the ISS and culturing on board for 3 days did not affect cell proliferation or apoptosis, but severely modified vimentin organization

Some key cellular parameters that we first evaluated after the flight are shown in Fig. 2. The transfer of ARPE-19 cells (treated or not treated with CoQ10) to the ISS and the 3 days of incubation on board had no impact on their proliferation rate compared to ground controls. In both cases, the cells almost reached confluence and did not show any signs of damage (Fig. 2A) or apoptosis, as assessed by the TUNEL assay (Fig. 2B). However, as indicated in the representative images of immunofluorescence microscopy analysis in Fig. 2C, the organization of the vimentin network underwent profound alterations, including a marked increase in its localization in the cellular perinuclear area and a concomitant redistribution from the cellular borders, which emphasized the collapse of the vimentin intermediate filament network.

### Transferring ARPE-19 cells to the ISS and culturing on board for 3 days dramatically modified the transcriptome profile

We then explored the possibility that spaceflight alters gene expression by analyzing ARPE-19 transcriptome profiles with respect to ground controls using next-generation sequencing technology, assuming a threshold of 0.05, for statistical significance ( $p$  value) and a change in the expression of a log fold with an absolute value of at least 1. Of 23,556 genes analyzed, 5555 were DE after spaceflight with respect to the ground controls (Fig. 3A and Supplementary S1). Among them, 3081 were upregulated and 2474 were downregulated. To predict the impact of the ISS environment on ARPE-19 gene expression pathways, we used the iPathwayGuide to assess the possibility that a specific pathway was perturbed and that the subsequent genes in a pathway were significantly more perturbed than the previous ones. The results predicted that 99 pathways defined in the KEGG database were significantly affected (Fig. 3B and Supplementary S2). The first ten pathways are shown in Table 1, and pathway diagrams containing coherent cascades and DE pathway genes are presented in Supplementary S3A-I. The most significantly impacted pathways were related to cellular responses to space environment adaptation/damage. The analysis of DE genes associated with perturbed pathways revealed down-modulation of metabolic pathways, N-Glycan biosynthesis, protein processing in the endoplasmic reticulum, p53 signaling, cellular senescence, mitophagy, and steroid biosynthesis, and up-modulation of MAPK, TGF-beta, and Rap1 signaling (Fig. 3C). To further explore the functional roles of the DE genes, we performed

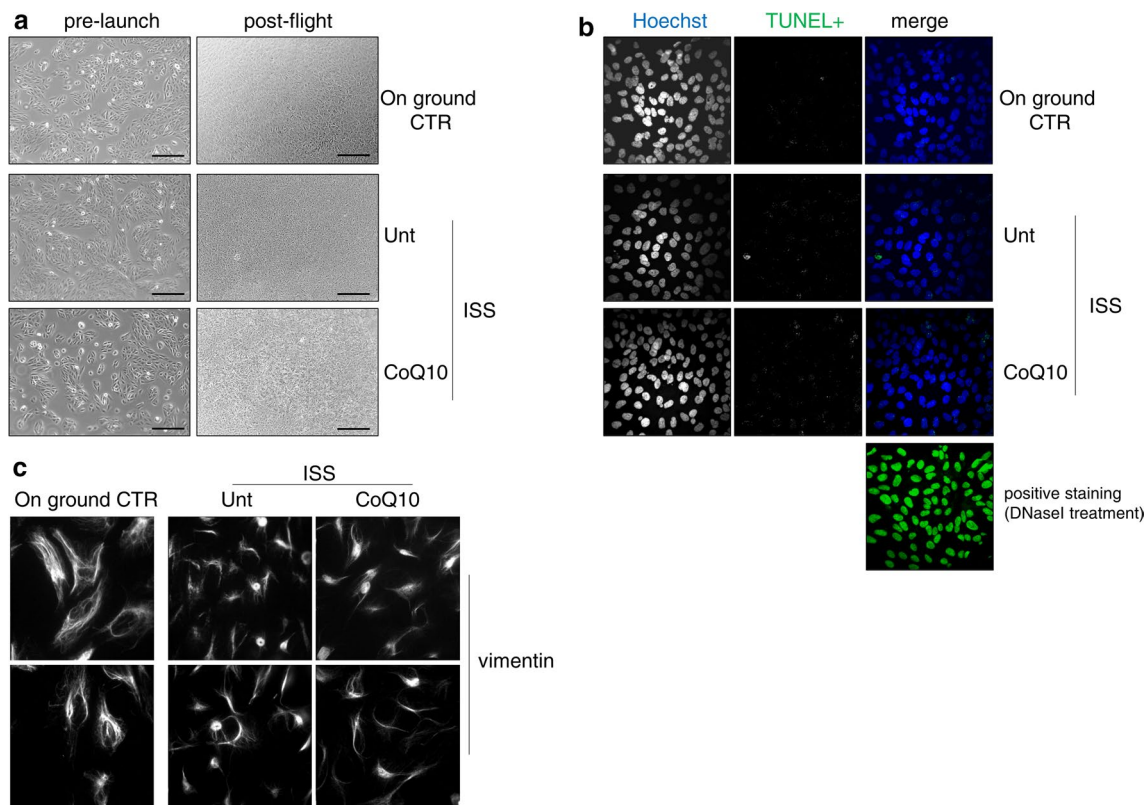


**Fig. 2** **A** Representative photomicrographs obtained with phase-contrast microscopy in ARPE-19 cells pre-launch and post-flight. Scale bar: 200  $\mu\text{m}$ . **B** Evaluation of apoptosis in ARPE-19 cells by

TUNEL fluorescent staining. Image size: 250  $\times$  250  $\mu\text{m}$ . **C** Evaluation of vimentin cellular localization in ARPE-19 cells by immunofluorescence. Image size: 100  $\times$  100  $\mu\text{m}$

GO analysis (Fig. 4 and Supplementary S4), which demonstrated that the transfer of ARPE-19 cells to the ISS and their culturing for 3 days on board caused an alteration in response to unfolded protein, stress response of the endoplasmic reticulum, and ion binding. The first five GO terms in biological processes, molecular functions, and cellular components are listed in Table 2.

The presence of lncRNAs was screened among the DE genes, based on the lncRNAs noted on the HUGO Gene Nomenclature Committee website, which included a total of 4118 lncRNAs (<http://www.genenames.org/cgi-bin/statistics>) (Supplementary S5). The expression of 255 lncRNAs was deregulated in ARPE-19 cells cultured on board the ISS; 208 were upregulated and 47 were downregulated (the top ten up- and down-regulated lncRNAs are presented in Table 3). To predict active micro-RNAs (miRNAs) in ARPE-19 cells cultured on board the ISS compared to ground control, the DE genes were also analyzed to determine the presence of enriched DE targets of the miRNAs. For a given miRNA, the analysis computed the ratio between the number of DE targets and all differentially expressed targets and compared it with the ratio

of all targets expressed downwards with all targets. This allowed for the calculation of the probability of observing a greater number of differentially downregulated target genes for a given miRNA only by chance. Of a total of 366 screened miRNAs, 19 achieved significant expression values, as described in Fig. 5 and Supplementary S6, with *hsa-miR-296-5p*, *hsa-miR-494-3p*, and *hsa-miR-128-3p* showing the best *p* values.

We then evaluated the role of CoQ10 treatment on gene expression in ARPE-19 cells cultured on board the ISS. Assuming a threshold of 0.05 for *p* and of 0.4 for fold change, of the 26,694 genes analyzed, we found 153 DE genes in cells treated with CoQ10 with respect to untreated controls (Fig. 6A and Supplementary S7). Among these DE genes, 81 were upregulated and 72 were downregulated in spaceflight ARPE-19 cells. iPathwayGuide analysis predicted that 22 pathways defined in the KEGG database were significantly affected (Fig. 6B and Supplementary S8), among which type I diabetes mellitus, HIF-1 signaling, ferroptosis, and Notch signaling pathways were the most significantly affected.

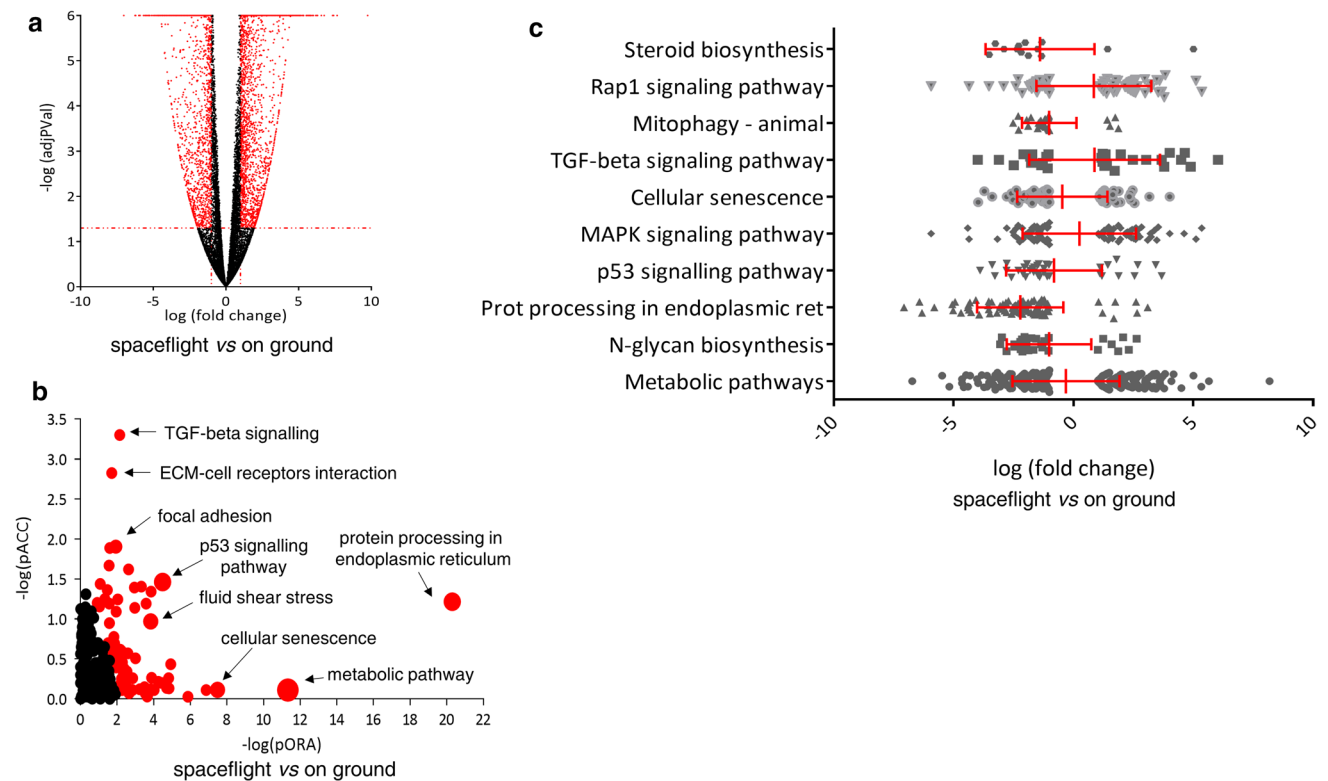


**Fig. 3** Gene expression analysis of ARPE-19 cells cultured on board the International Space Station compared to on ground. **A** The 5555 significantly differentially expressed (DE) genes (shown in red) are represented in the Volcano plot in terms of their measured expression change (x-axis) and the significance of the change (y-axis). The significance is represented in terms of the negative log (base 10) of the *p* value, such that genes that are more significant are plotted higher on the y-axis. The dotted lines represent the thresholds used to select the DE genes: 1 for expression change and 0.05 for significance. **B** Pathways perturbation vs over-representation: the pathways are plotted

in terms of the two types of evidence computed by iPathwayGuide: over-representation is on the x-axis (pORA) and the total pathway accumulation is on the y-axis (pAcc). Each pathway is represented by a single dot, with significant pathways shown in red, non-significant in black, and the size of each dot is proportional to the size of the pathway it represents. Both *p* values are shown in terms of their negative log (base 10) values. **C** DE pathway genes of the most significant impacted pathways. The mean value and standard deviation are indicated in red

**Table 1** Most significantly affected pathways in ARPE-19 cells cultured on board ISS compared to on ground

Pathway name	Pathway ID (KEGG)	<i>p</i> -value	<i>p</i> -value (FRD)	<i>p</i> -value (Bonferroni)
Metabolic pathways	01,100	4.716e-12	1.504e-9	1.504e-9
N-Glycan biosynthesis	00,510	1.374e-7	2.192e-5	4.385e-5
Protein processing in endoplasmic reticulum	04,141	1.074e-6	1.142e-4	3.426e-4
p53 signaling pathway	04,115	1.160e-5	9.248e-4	0.004
MAPK signaling pathway	04,010	1.649e-5	9.861e-4	0.005
Cellular senescence	04,218	1.855e-5	9.861e-4	0.006
TGF-beta signaling pathway	04,350	4.917e-5	0.002	0.016
Mitophagy—animal	04,137	5.734e-5	0.002	0.018
Rap1 signaling pathway	04,015	8.164e-5	0.003	0.026
Steroid biosynthesis	00,100	9.600e-5	0.003	0.031

**Fig. 4** Gene Ontology analysis of differentially expressed genes in ARPE-19 cells cultured on board the International Space Station compared to on ground. The top ten Gene Ontology (GO) terms in biological processes (green), molecular functions (red), and cellular components (blue) category are listed

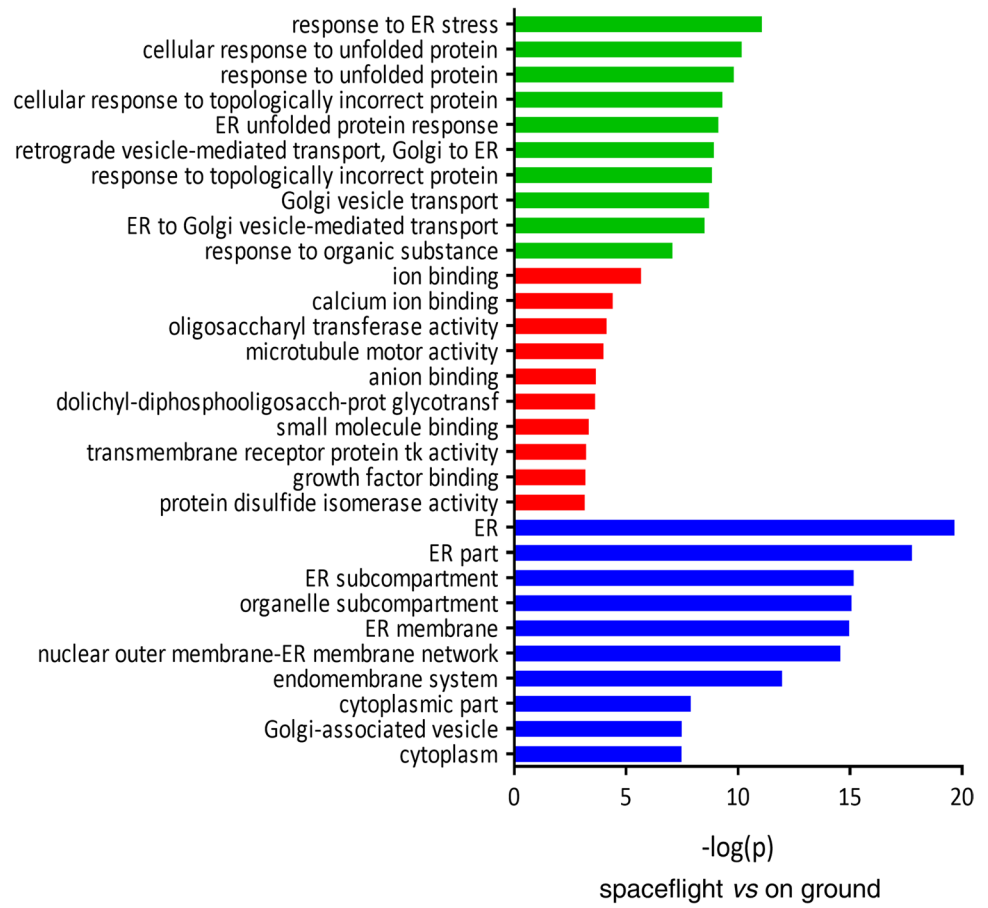


**Table 2** GO analysis

Category	Identifier	Description	Count DE	Count All	<i>p</i> -value	<i>p</i> -value (FDR)	<i>P</i> -value (Bonferroni)
Biological Processes	GO:0,034,976	Response to endoplasmic reticulum stress	125	261	1,10e-11	1,29e-02	1,29e-02
	GO:0,034,620	Cellular response to unfolded protein	72	130	7,40e-11	4,34e-02	8,68e-02
	GO:0,006,986	Response to unfolded protein	86	167	1,80e-10	7,04e-03	2,11e-06
	GO:0,035,967	Cellular response to topologically incorrect protein	77	147	5,80e-10	1,70e-06	6,80e-06
	GO:0,030,968	Endoplasmic reticulum unfolded protein response	67	123	8,70e-10	2,04e-06	1,02e-05
Molecular Functions	GO:0,043,167	Ion binding	1715	5615	2,50E-06	7,34E-03	7,34E-03
	GO:0,005,509	Calcium ion binding	217	610	4,60E-05	1,00E+00	1,00E+00
	GO:0,004,576	Oligosaccharyl transferase activity	9	10	8,80E-05	1,00E+00	1,00E+00
	GO:0,003,777	Microtubule motor activity	39	81	1,20E-04	1,00E+00	1,00E+00
	GO:0,043,168	Anion binding	784	2509	2,60E-04	1,00E+00	1,00E+00
Cellular Components	GO:0,005,783	Endoplasmic reticulum	616	1615	2,40E-20	3,33e-13	3,33e-13
	GO:0,044,432	Endoplasmic reticulum part	463	1173	2,10E-18	1,46e-10	2,92e-11
	GO:0,098,827	Endoplasmic reticulum Subcompartment	372	931	7,60E-16	3,16e-07	1,06e-07
	GO:0,031,984	Organelle subcompartment	554	1489	9,10E-16	3,16e-07	1,26e-07
	GO:0,005,789	Endoplasmic reticulum membrane	370	928	1,30E-15	3,61e-09	1,81e-08



**Table 3** Top ten up- and downregulated lncRNAs in ARPE-19 cultured on board ISS

ID symbol	lncRNA name	Chromosome location RefSeq accession	Description	Expression (log fc)
HGNC:44,153	<i>DIO2-AS1</i>	14q31.1 NR_038355	DIO2 antisense RNA 1	6,3
HGNC:27,121	<i>LINC00906</i>	19q12 NR_027318	Long intergenic non-protein coding RNA 906	5,4
HGNC:45,193	<i>PLCE1-AS1</i>	10q23.33 NR_033969	PLCE1 antisense RNA 1	5,2
HGNC:27,437	<i>WDR11-AS1</i>	10q26.12 NR_033850	WDR11 antisense RNA 1	5,1
HGNC:48,727	<i>LINC00968</i>	8q12.1 NR_038236	Long intergenic non-protein coding RNA 968	4,7
HGNC:42,692	<i>LINC00370</i>	13q33.3 BF695150	Long intergenic non-protein coding RNA 370	4,6
HGNC:27,471	<i>TRHDE-AS1</i>	12q21.1 NR_026836	TRHDE antisense RNA 1	4,6
HGNC:40,587	<i>TM4SF1-AS1</i>	3q25.1 NR_046650	TM4SF1 antisense RNA 1	4,5
HGNC:49,095	<i>CLSTN2-AS1</i>	3q23 NR_108084	CLSTN2 antisense RNA 1	4,4
HGNC:44,989	<i>LINC00842</i>	10q11.22 NR_033957	Long intergenic non-protein coding RNA 842	4,4
HGNC:44,064	<i>SLC7A11-AS1</i>	4q28.3 NR_038380	SLC7A11 antisense RNA 1 non-coding RNA	- 3,1
HGNC:40,792	<i>ARHGAP26-AS1</i>	5q31.3 NR_046680	ARHGAP26 antisense RNA 1	- 3,1
HGNC:48,575	<i>LINC00888</i>	3q27.1 NR_038301	Long intergenic non-protein coding RNA 888	- 3,1
HGNC:41,429	<i>ARHGAP26-IT1</i>	5q31.3 NR_046816	ARHGAP26 intronic transcript 1 non-coding RNA	- 3,3
HGNC:17,263	<i>PART1</i>	5q12.1 AF16347	Prostate te androgen-regulated transcript 1	- 3,4
HGNC:48,498	<i>LUCAT1</i>	5q14.3 NR_103548	Lung ancer associated transcript 1	- 3,5
HGNC:48,574	<i>LINC00887</i>	3q29 NR_024480	Long intergenic non-protein coding RNA 887	- 3,9
HGNC:23,135	<i>RN7SL3</i>	14q21.3 NG_011406	RNA component of signal recognition particle 7SL3	- 4,6
HGNC:4713	<i>H19</i>	11p15.5 NR_002196	H19 imprinted maternally expressed transcript	- 4,6
HGNC:42,812	<i>MRPL23-AS1</i>	11p15.5 NR_024471	MRPL23 antisense RNA 1	- 5,8

## Discussion

In the present study, we investigated the impact of the space environment on human retinal pigment epithelial cells. For this purpose, ARPE-19 cells were transferred and cultured for 3 days onboard the ISS; in addition, cells were cultured in the presence or absence of CoQ10. As a control, ARPE-19 cells were cultured on the ground under normal conditions.

Previous ground experiments on ARPE-19 cells using microgravity simulators have led to contrasting results. We previously showed that 3 days of simulated microgravity

obtained by the rotating wall vessel bioreactor (RWV) increased the activity of caspase 3/7 and reduced the mitochondrial transmembrane potential, which is evidence of apoptosis induction [26]. In contrast, using a different microgravity simulator (random positioning machinery, RPM), Corydon et al. did not report apoptotic events in ARPE19 cells cultured for 5–10 days under simulated microgravity conditions [34]. In the present study, we found that the transfer of ARPE-19 cells from Cape Canaveral to the ISS and 3-day incubation on board did not affect their proliferation rate nor induce apoptosis with respect to the ground

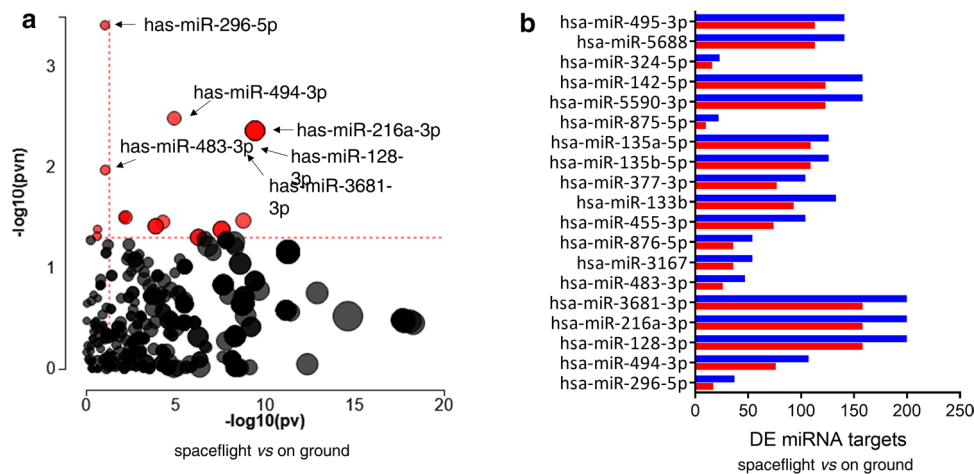


**Fig. 5** Bioinformatics miRNA analysis in ARPE-19 cells cultured on board the International Space Station compared to on ground. **A** Significant differences in the expression of specific miRNAs plotted in terms of the two types of evidence computed by iPathwayGuide: the x-axis ( $-\log_{10}(pv)$ ) represents the  $p$  value based on the total number of differentially expressed (DE) target genes versus the total number of target genes and the y-axis ( $-\log_{10}(pvn)$ ) is the  $p$  value based on

the number of downregulated DE targets versus the total number of DE miRNA targets. Each miRNA is represented by a single dot, with significant miRNAs shown in red, non-significant in black, and the size of each dot is proportional to the size of the number of target genes for that miRNA relative to others. **B** List of the 19 miRNAs that reached significance, depicting the number of DE target genes that are under- (in blue) or over-expressed (in red)

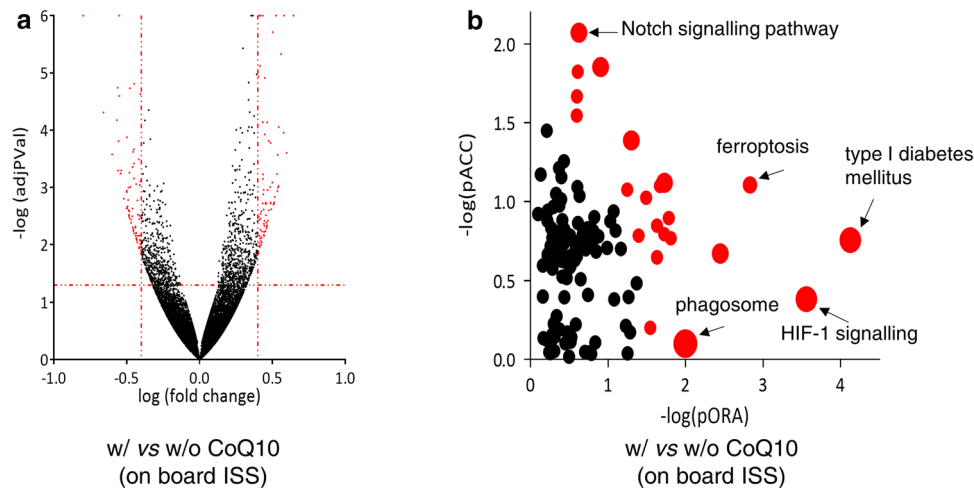


**Fig. 6** Gene expression analysis of ARPE-19 cells cultured on board the International Space Station in the presence of absence of coenzyme Q10. **A** All 153 significantly differentially expressed (DE) genes (showed in red) are represented in the Volcano plot in terms of their measured expression change (x-axis) and the significance of the change (y-axis), as in Fig. 3A. The dotted lines represent the thresh-

olds used to select the DE genes: 0.4 for expression change and 0.05 for significance. **B** Pathway perturbation vs over-representation. Each pathway is represented by a single dot, with significant pathways shown in red, non-significant in black, and the size of each dot is proportional to the size of the pathway it represents. Both  $p$  values are shown in terms of their negative log (base 10) values

controls (Fig. 2A, B). These results could be explained by differences between microgravity simulated by the available simulator devices and between simulated microgravity and real microgravity onboard the ISS, and the use of these devices and the impact of flight hardware on cellular physiology are currently debated [35, 36]. Cells living

onboard the ISS are simultaneously subjected to microgravity and space radiation, which typically do not occur in on-ground simulation experiments, where the two treatments are administered separately [37]. Indeed, the constant threat to the integrity of astronauts represented by space radiation, which causes damage to DNA directly or via the production

of free radicals, and microgravity, which hampers DNA repair, have raised the opportunity to explore the potential synergies between microgravity and radiation, both in space and in Earthly analogs. The results have been conflicting, which indicates the need to perform experiments in a space environment [37]. Furthermore, in our experiment, the 3-day culturing of ARPE-19 cells on board the ISS was preceded by a 5-day permanence into the Biokit at a relatively low temperature (up to approximately 26 °C). It has been demonstrated that hypothermia elicits a strong expression of cold shock proteins in mammalian retinal cells, including retinal pigment epithelial cells [38], where they may act as protective factors against damage and prevent apoptosis [39]. Finally, it should be noted that, in our experiment, ARPE-19 cells were cultured inside the KUBIK on board the ISS for 3 days, however, due to the transfer from the ground to the ISS, the cells underwent microgravity conditions several hours before entering the KUBIK, which could have affected adaptive behavior.

Cytoskeletal disorganization and significant changes in the expression of its main components, actin, tubulin, and vimentin, both at phenotypic and genotypic levels, have been observed in various cell types subjected to altered gravity conditions [40–43] and complete destruction of the microtubule network was observed in Jurkat cells following exposure to real microgravity [44]. Similarly, in endothelial cells, a significant reduction in actin fibers was observed in response to simulated microgravity [45] and a significant increase in stress fibers following hypergravity [46]. ARPE-19 cells cultured for 5 days and 10 days on RPM revealed the appearance of two major phenotypes, i.e., adherent monolayers and 3D multicellular spheroids [34]. In addition, the reduction of F-actin filaments in favor of F-actin structures at the cell boundaries, and the downregulation of *beta-actin*, *beta-tubulin*, *keratin 8*, *vimentin*, *laminin subunit beta 2*, *integrin beta 1*, *integrin beta 3*, and *collagen 4* gene expression have been revealed, suggesting that simulated microgravity reduces the ability of exterior structures in ARPE-19 cells to retain adhesion and stiffness [34]. Other cell types differ from ARPE-19 cells in their cytoskeleton-related responses to microgravity. For example, RPM induces the upregulation of *beta actin* gene expression in MCF-7 breast carcinoma [47] and in human primary chondrocytes [48] and of *vimentin* gene expression in FLG 29.1 leukemic cells [46] and ML-1 follicular thyroid carcinoma cells [49]. Here, we revealed a dramatic change in the cytoskeletal vimentin distribution in ARPE-19 cultured for 3 days onboard the ISS. Vimentin is a cytoskeletal protein responsible for maintaining cellular integrity and is the main constituent of intermediate filaments, which provide structural support for the cytoplasm and play an essential role in the response to mechanical stresses, such as gravity [50]. Recently, it has been demonstrated that the vimentin

network maintains the resilience of the cytoplasm and enhances cytoplasmic mechanical strength and toughness under dynamic deformation via poroelastic and viscoelastic relaxation [51]. Thus, vimentin networks may reduce the risk of cell damage during major deformation events [51]. In our study, immunofluorescence analysis revealed deregulated vimentin cellular localization, mostly concentrated in the perinuclear region in cells exposed to real microgravity (Fig. 2C). The different distribution of vimentin in cells exposed to microgravity compared to the control denotes a change in the shape of the cells and suggests an alteration in the capability of cells to interact with others and with extracellular matrix components. Moreover, vimentin analysis revealed that spaceflight ARPE-19 cells contained perinuclear structures resembling aggresomes. Aggresomes are protein inclusions aggregates at the centrosome-nuclear bay, and contain proteins destined to degradation that are located within a cage comprised of intermediated filament, including vimentin [50, 52]. The formation of aggresomes is directly linked to disruption of proper protein homeostasis, in particular when elevated levels of misfolded or damaged proteins accumulate into cells [50]. This observation suggests that the real microgravity determines an alteration of protein processing in ARPE-19 cells, and is consistent with the following transcriptomic data.

The first observation that microgravity altered gene expression occurred > 20 years ago; however, since the most apparent detrimental effect of long-lasting space flights on astronauts was the strong atrophy of their musculoskeletal system, studies mainly focused on gene expression in bone and muscle cells. Subsequently, several studies have highlighted the impact of the spatial environment on gene expression in different tissues, but the real milestone for high-performance studies of the expression of entire panels of genes in response to spatial radiation and microgravity has been the recent application of genomic and proteomic approaches. Understanding the variations in gene expression in their maximum amplitude is key to unraveling the pathogenesis of damage endured by astronauts during spaceflight and, ultimately, to identify effective countermeasures. The present study found a considerable number of upregulated and downregulated DE genes (Fig. 3A). KEGG analysis, impact analysis, and GO annotation revealed that several relevant biological pathways and cellular functions were affected by space flight (Fig. 3B, C, Fig. 4). Among them, protein processing in the endoplasmic reticulum (ER) is one of the most impacted, which is also justified by the vimentin network alterations described above. The ER is a complex endomembrane system in which proteins are folded and transported to distinct cellular districts [53]. Correctly folded proteins are packaged into transport vesicles and shuttled into the Golgi system. Misfolded proteins are retained within the ER, coupled with chaperones, and if terminally misfolded,

subjected to ER-associated degradation. ER accumulation of misfolded proteins determines ER stress and evokes the unfolded protein response (UPR), which aims to inhibit protein translation, degrade misfolded proteins, increase chaperone production, and eventually induce apoptosis [53]. ER stress and UPR have been correlated with microgravity in different cell types [54–56]. We found that the majority of DE genes involved in this pathway were downregulated in ARPE-19 cells cultured onboard the ISS. However, some members of the 70 kDa heat shock protein (*HSP70*) gene family (*HSPA1A*, *HSPA8*, and *HSPA2* in particular) and E3 ligase parkin (*PARK2*) genes, which are involved in chaperone and E3 ubiquitin ligase activity, respectively, were significantly upregulated. Recently, interesting studies have been conducted on human endothelial cells (HUVECs). It has been reported that 4 days of HUVEC culture in RWV simulated microgravity-induced cell stress and promoted *HSP70* upregulation, likely sustaining the early phases of the dynamic adaptation of HUVECs to microgravity, while *HSP70* silencing impaired cell survival [57]. In addition, reduced mitochondrial function and mitochondrial content have been demonstrated [57], and the contribution of mitophagy to this adaptation, which culminates in a thrifty phenotype, has been demonstrated [41]. In addition to its role in ER metabolism, Parkin is a central regulator of mitophagy [58], another pathway found to be significantly impacted in ARPE-19 cells cultured onboard the ISS. Deteriorous byproducts or oxidative stress lead to mitochondrial dysfunction, which, if the damage is unrepairable, culminates in mitochondria recognition and targeting for degradation via the autophagic process termed mitophagy [58]. Multi-omics analysis recently identified mitochondrial dysregulation as a central biological hub for the pathophysiological effects of spaceflight [59]. In this context, Parkin recognizes altered proteins on the mitochondrial outer membrane and mediates damaged mitochondrial clearance [58]. Microphthalmia-associated transcription factor (*MITF*) is another gene belonging to the mitophagy pathway [60] that is upregulated in ARPE-19 cells exposed to the space environment. *MITF* is a transcription factor responsible for retinal pigment epithelial cell development and function [61]. *MITF* plays a protective role against oxidative stress in ARPE-19 cells, where it upregulates antioxidant gene expression and mitochondrial biogenesis, mainly via peroxisome proliferator-activated receptor-gamma coactivator 1 alpha (*PGC1a*) and nuclear factor erythroid 2-related factor 2 (*NRF2*) upregulation [62].

In our experiment, transforming growth factor (TGF)-beta and p53 signaling were deregulated in ARPE-19 cells cultured onboard the ISS. While most of the DE genes involved in TGF-beta signaling were upregulated, the opposite was true for p53 signaling. Using a system biology approach to evaluate rodent transcriptomic data from

GeneLab (Genelab.nasa.gov), TGF-beta and p53 were identified as the most prevalent pan-tissue signaling pathways activated in response to microgravity [63]. p53 is a major contributor to cell cycle arrest, DNA repair, and apoptosis induction in response to genotoxic or non-genotoxic damage [64]. p53 signaling is frequently activated in response to microgravity. However, heterogeneous responses have been observed depending on the cell type and culture conditions. For example, p53 pathway activation has been recently described in macrophages undergoing spaceflight or RWV simulated microgravity [65] and in lung cancer cells cultured with RPM [66], while the inhibition of p53 signaling under 3D-clinostat simulated microgravity was found in hepatoblastoma cells [67]. In ARPE-19 cells cultured onboard the ISS, we detected several p53-transactivated pro-apoptotic genes (e.g., *BAX*, *PMAIP1*, *BBC3*), and genes involved in cell cycle arrest (e.g., *CDKN1A*, *GADD45A*, *GADD45B*) and DNA repair and damage prevention (*DDB2*, *GADD45A* [67], *GADD45B*, *SESN2*) were downregulated. Similarly, we found that cellular senescence pathway genes, and in particular, most of the genes encoding senescence-associated secretory phenotype (SASP) factors [68], such as *IL1A*, *CXCL8*, *SERPINE1*, and *IGFBP3*, were significantly downregulated. In contrast, the gene coding for the SASP TGF-beta factor was upregulated. TGF-beta is a master regulator that coordinates the systemic response to microgravity at multiple biological scales [63]. TGF-beta is a well-known cytokine that belongs to a family of several protein members, including bone morphogenic proteins, growth differentiation factors, activins, and inhibins, all of which regulate a wide spectrum of cellular functions such as proliferation, apoptosis, differentiation, and immune responses [69]. TGF-beta plays a major role in retinal pigment epithelial cells, particularly in a dynamic transition along a well-differentiated, polarized epithelial to mesenchymal cells, which has been defined as retinal pigment epithelium dysfunction [70]. Functional retinal pigment epithelial cells form a single layer of polarized cells located between the photoreceptors and the choroid. Correct differentiation and polarization of the retinal pigment epithelium are essential for proper functioning. While epithelial features guarantee retinal pigment epithelium physiological homeostasis in the retina, different mechanisms have been found to be involved in retinal pigment epithelium epithelial to mesenchymal transition (EMT) and mesenchymal to epithelial transition (MET), which hinder their functions [70]. Microgravity has been previously demonstrated to trigger EMT in different cell types [65, 71]. TGF-beta signaling is one of the most potent EMT inducers and is, therefore, a major contributor to retinal pigment epithelium dysfunction [70]. High levels of vitreal TGF-beta have been detected in proliferative vitreoretinopathy patients, a pathological condition in which EMT of the retinal pigment epithelium plays an essential pathogenic role [72], which led to the evaluation

of TGF-beta signaling inhibitors able to counteract EMT for the treatment of proliferative retinal diseases such as proliferative vitreoretinopathy [73]. The Hippo signaling pathway is closely interconnected with that of TGF-beta, and in our experiment, it was significantly affected in ARPE-19 cells cultured on board the ISS. This pathway regulates retinal pigment epithelial cell differentiation and is involved in EMT [74]. Connective tissue growth factor (*CTGF*) encodes a cysteine-rich extracellular matrix protein that acts downstream of the TGF-beta and Hippo signaling pathways [75, 76]. We found that *CTGF* is one of the genes overexpressed in ARPE-19 cells cultured on board the ISS. It has been hypothesized that its binding to various cell surface receptors, including integrin receptors, heparan sulfate proteoglycans, and low-density lipoprotein receptor-related proteins, enables CTGF to regulate key cellular functions, such as cell adhesion, proliferation, chemotaxis, differentiation, survival, and extracellular matrix component production [77]. A previous study indicated that CTGF increases the migratory ability of retinal pigment epithelial cells and that it is a major mediator of retinal fibrosis [78]. In addition, it has been recently demonstrated that the Hippo pathway is severely altered in a murine model of retinal degeneration, in which *CTGF* is markedly upregulated [76].

Analysis of DE genes revealed deregulation of the expression and activity of lncRNAs (Table 3 and Supplementary S5) and microRNAs (Fig. 5 and Supplementary S6), respectively, in ARPE-19 cells. LncRNAs are defined as transcripts longer than 200 nucleotides that generally lack protein-coding potential and can be processed like mRNAs, i.e., spliced and polyadenylated [79]. LncRNAs are involved in several cellular physiological processes, such as adaptation to stress, cell differentiation, maintenance of pluripotency, and apoptosis [79]. The correct balance of lncRNA levels is crucial for the maintenance of cellular equilibrium, and their dysregulation is associated with many disorders [79]. Variations in lncRNA expression have been documented in different cell types exposed to simulated microgravity [80–82]. Here, we demonstrated that real microgravity alters a panel of lncRNAs in ARPE-19 cells, most of which were upregulated. Considering the top ten up- and down-regulated lncRNAs, the only one involved to date in retinal cell physiology is *H19*, which is involved in retinal cell death and in the inflammatory response of ARPE-19 cells exposed to hyperglycemia [83]. We detected strong downregulation of *H19* expression in ARPE-19 cells cultured onboard the ISS, and it has been reported that *H19* downregulation correlates with TGF-beta-mediated EMT in retinal endothelial cells [84]. Similarly, another two lncRNAs downregulated in ARPE-19 cells cultured onboard the ISS, namely *SLC7A11-AS1* and *LUCAT1*, are reported to be involved in the EMT process [85, 86]. MicroRNAs are small single-stranded non-coding RNAs, whose functions in RNA silencing

and post-transcriptional regulation of gene expression are well-known [87, 88]. A recent milestone study identified a spaceflight-associated microRNA signature in response to simulated short- and long-duration spaceflight and simulated deep-space radiation conditions [89]. In addition, the panel of spaceflight-associated microRNAs has been predicted to interfere with cell signaling and metabolic pathways, partly through interaction with TGF-beta signaling [63]. Some microRNAs that were identified to be activated in ARPE-19 cells cultured on board the ISS are involved in the cell response to spaceflight. Among them, *hsa-miR-296* expression was affected in HUVECs cultured in a 3D clinostat to simulate microgravity and was found to influence cell proliferation and vascular function under microgravity conditions [90]. *hsa-miR-494* is upregulated in C2C12 myoblast cells subjected to clinorotation conditions and in osteoblasts isolated from tail-suspended rats, and this upregulation correlates with the inhibition of osteoclast differentiation [91]. Other miRNAs we identified are involved in the EMT process. For example, *hsa-miR-145-3p*, *hsa-miR-324-5p*, and *hsa-miR142-5p* act as inhibitors of EMT in different cell types [92–95]; in contrast, high expression and activation of *hsa-miR 483-3p*, *hsa-miR-128-3p* are involved in EMT induction.

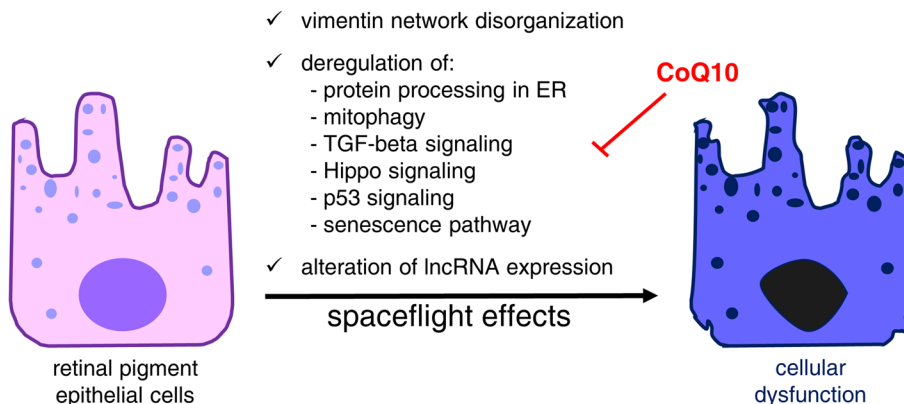
CoQ10 is an essential cofactor in the electron transport chain. It is endowed with well-known protective actions with respect to different types of damage on various cell types, including those of the retina, which mainly depends on its free radical scavenging ability and the regulation of the mitochondrial permeability transition pore [29]. It is known that the choroid/retina levels of endogenous CoQ10 decrease with aging concomitantly with the progression of apoptosis-related retinal diseases [96]. We previously demonstrated the efficacy of the topical administration (via eye drops) of CoQ10 to protect retinal cell layers commissioned to apoptosis by a variety of noxious stimuli [27, 28]. On these bases, we tested the role of CoQ10 treatment in modulating the transcriptome of ARPE-19 cells cultured onboard the ISS. We found a limited number of DE genes that were subjected to KEGG and impact analyses (Fig. 6). Among the most affected biological pathways affected by CoQ10 treatment, we focused on HIF-1 signaling and ferroptosis. HIF-1 is a well-known transcription factor discovered by virtue of its role as a master regulator of oxygen homeostasis [97]. HIF-1 signaling is involved in numerous cellular responses to a variety of environmental stresses. Interestingly, it has been demonstrated that, regardless of its function as a transcription factor, HIF-1 has a protective role through its localization into mitochondria, where it reduces reactive oxygen species levels and reverses mitochondrial damage [98]. Previous studies have revealed that microgravity affects HIF-1 pathway activation. Wang et al. demonstrated that 28 days of simulated microgravity induced oxidative stress and HIF-1

activation and a panel of its downstream targets in rat hippocampus, while Vogel et al. demonstrated that *HIF-1a*- and HIF-1-dependent transcripts were differentially regulated under altered gravity on monocytes and macrophages during parabolic flight and suborbital ballistic rocket campaigns, whereas HIF-1-dependent gene expression adapted after 5 min of microgravity [99]. Ferroptosis is a peculiar type of iron-dependent cell death; it was first characterized in 2012 and results from the accumulation of toxic levels of lipid-reactive oxidative species [100]. Increased intracellular iron accumulation is a classical ferroptosis activator that is directly linked to the failure of glutathione (GSH)-dependent antioxidant defenses. Cellular iron metabolism includes absorption of the ferritin-Fe<sup>3+</sup> complex by the transferrin receptor (TFRC), and it has been demonstrated that reducing iron utilization may increase the sensitivity to ferroptosis [101]. GSH production is sustained by the activity of the amino acid antiporter, SLC7A11/xCT/system xc<sup>-</sup>, which guarantees the exchange of extracellular cystine (which, in turn, generates cysteine, a limiting precursor for GSH synthesis) for intracellular glutamate [100]. It is known that inhibition of system xc<sup>-</sup> causes GSH depletion to trigger ferroptosis [102]. The direct involvement of CoQ10 in ferroptosis has been recently reported. It is known that the reduced form of CoQ10 is a potent antioxidant that counteracts lethal lipid peroxidation, thus acting as a ferroptosis suppressor. In particular, the NADH-dependent oxidoreductase, FSP1, converts non-mitochondrial oxidized to reduced CoQ10, thus furnishing a GSH-independent protective axis to counteract membrane lipid peroxidation [103]. In addition to this role, we found that CoQ10 treatment of ARPE-19 cells cultured on board the ISS reduced *TFRC* and induced *SLC7A11* gene expression, corroborating the evidence that CoQ10 acts as a direct ferroptosis inhibitor and *bona fide* increases ferroptosis resistance by reducing iron cellular uptake and enhancing cystine uptake.

## Conclusion

Our results indicate that the transfer of cultured ARPE-19 human retinal cells to the ISS and their 3-day living on board severely altered cytoskeleton morphology and the transcriptome profile, indicating the emergence of cellular dysfunction (Fig. 7). Although obtained in a single experiment, in which we were able to use only a limited number of ARPE-19 cells in culture to carry out the various analyses, we suggest that our results may, at least partially, reflect the response of the retinal pigment epithelial cells of astronauts' eyes subjected to space flight. The retinal pigment epithelium has peculiar functions strictly linked to its structure that are essential for normal vision [104]. Alterations in retinal pigment epithelium physiology can lead to retinopathy, which consequently affects vision. Retinal pigment epithelium dysfunction is known to be involved in the pathogenesis of several degenerative retinal diseases including age-related macular degeneration, retinitis pigmentosa, and Stargardt disease [105]. Moreover, retinal pigment epithelium dysfunction accompanies the course of non-degenerative retinal diseases, such as diabetic retinopathy [106], and is of primary importance in proliferative diseases such as proliferative vitreoretinopathy [70]. The results obtained in the present study, highlighting the potential dysfunction of ARPE-19 cells, are consistent with what has been observed *in vivo* in previous studies in rodents housed in spacecraft for several days [16, 107]. Interestingly, during the same SpaceX CRS-12 mission as our experiment, retinal pigment epithelium thickness reduction was observed in the retinas of mice hosted for 40 days on board the ISS [107]. Therefore, although the evidence we report here does not have an immediate impact on SANS pathogenesis, it poses an alert for the health of the astronauts' retinas, particularly in view of long-term missions, which may even extend to years. Approximately 60% of astronauts returning from long-term missions exhibit signs of SANS, the etiology of which is currently debated [19]. The causes of SANS are thought to be a mild and chronic increase in intracranial pressure, congestion

**Fig. 7** Effects of space flight on ARPE-19 cells. The conclusions reported in the picture, except that relative to vimentin network disorganization, are based on transcriptomic data



of cerebral venous, and alteration of folate-dependent 1-carbon metabolism [23]. Regardless of its causes, reducing the risk of SANS is a priority for long-term spaceflight planning. Among the signs of SANS, two are particularly feared. The first is optic disc edema, which may cause severe vision loss due to the occurrence of increasing blind spots. The second is retinal and choroidal folds, which, if severe and located near the fovea, can cause distortions or visual acuity reduction [108]. The contribution of spaceflight-dependent cellular alterations of individual retinal cell types in the pathogenesis of SANS has not yet been defined. However, results from experiments conducted on cell cultures suggest that the molecular and cellular responses to microgravity and radiation could synergize with macroscopic tissue and organ alterations in the pathogenesis of SANS. A recent example of this hypothesis comes from the observation that choroidal folds in the retina of a crewmember > 5 years post-flight induced alterations in the retinal pigment epithelium [108]. Therefore, the results presented herein suggest a rational basis for future investigations aimed at identifying effective countermeasures against SANS. On this line of evidence, the treatment of ARPE-19 cells with CoQ10 on board reveals its potential to increase cell resilience towards harmful agents in the space environment. Moreover, it can be hypothesized that at least some of the gene deregulations we found in ARPE-19 cells occur in other cell types and tissues of astronauts. Based on this assumption, the evidence that important cell pathways are significantly affected by spaceflight and, if deregulated, play a central role in a variety of severe human disorders, such as cancer, cardiovascular diseases, and diabetes, confirms possible connections to astronauts' health [109, 110].

**Supplementary Information** The online version contains supplementary material available at <https://doi.org/10.1007/s00018-021-03989-2>.

**Funding** This project was coordinated and funded by the Italian Space Agency (ASI, grant 2016–6-U0 to M.L.) for space station experimentation within the national ISS utilization rights. The authors thank Fondazione Cassa di Risparmio Di Firenze (Italy) for financial support.

**Data availability** All data and material used are available in the author's labs.

**Code availability (software application or custom code)** Not applicable.

## Declarations

**Conflict of interest** The authors declare no conflicts of interest/competing interests.

**Ethics approval** Not applicable.

**Consent to participate** Not applicable.

**Consent for publication** Not applicable.

## References

- Demontis GC, Germani MM, Caiani EG, Barravecchia I, Passino C, Angeloni D (2017) Human pathophysiological adaptations to the space environment. *Front Physiol* 8:547
- Strollo F, Gentile S, Strollo G, Mambro A, Vernikos J (2018) Recent progress in space physiology and aging. *Front Physiol* 9:1551
- Stavnichuk M, Mikolajewicz N, Corlett T, Morris M, Komarova SV (2020) A systematic review and meta-analysis of bone loss in space travelers. *NPJ microgravity* 6:13
- Norsk P (2020) Adaptation of the cardiovascular system to weightlessness: Surprises, paradoxes and implications for deep space missions. *Acta Physiol (Oxf)* 228 (3):e13434.
- Crucian BE, Chouker A, Simpson RJ, Mehta S, Marshall G, Smith SM, Zwart SR, Heer M, Ponomarev S, Whitmire A, Fripiat JP, Douglas GL, Lorenzi H, Buchheim JJ, Makedonas G, Ginsburg GS, Ott CM, Pierson DL, Krieger SS, Baecker N, Sams C (2018) Immune system dysregulation during spaceflight: potential countermeasures for deep space exploration missions. *Front Immunol* 9:1437
- Grigoriev AI, Bugrov SA, Bogomolov VV, Egorov AD, Polyakov VV, Tarasov IK, Shulzhenko EB (1993) Main medical results of extended flights on space station Mir in 1986–1990. *Acta astronautica* 29 (8).
- Bradbury P, Wu H, Choi JU, Rowan AE, Zhang H, Poole K, Lauko J, Chou J (2020) Modeling the impact of microgravity at the cellular level: implications for human disease. *Front Cell Dev Biol* 8:96
- Beck M, Moreels M, Quintens R, Abou-El-Ardat K, El-Saghire H, Tabury K, Michaux A, Janssen A, Neefs M, Van Oostveldt P, De Vos WH, Baatout S (2014) Chronic exposure to simulated space conditions predominantly affects cytoskeleton remodeling and oxidative stress response in mouse fetal fibroblasts. *Int J Mol Med* 34(2):606–615
- Mao XW, Boerma M, Rodriguez D, Campbell-Beachler M, Jones T, Stanbouly S, Sridharan V, Nishiyama NC, Wroe A, Nelson GA (2018) Combined Effects of Low-Dose Proton Radiation and Simulated Microgravity on the Mouse Retina and the Hematopoietic System. Radiation research.
- Mao XW, Pecaout MJ, Stodieck LS, Ferguson VL, Bateman TA, Boussein M, Jones TA, Moldovan M, Cunningham CE, Chieu J, Gridley DS (2013) Spaceflight environment induces mitochondrial oxidative damage in ocular tissue. *Radiat Res* 180(4):340–350
- Kast J, Yu Y, Seubert CN, Wotring VE, Derendorf H (2017) Drugs in Space: Pharmacokinetics and Pharmacodynamics in Astronauts. *European journal of pharmaceutical sciences : official journal of the European Federation for Pharmaceutical Sciences* 109S.
- Eyal S, Derendorf H (2019) Medications in Space: In Search of a Pharmacologist's Guide to the Galaxy. *Pharm Res* 36 (10):148.
- Mao XW, Boerma M, Rodriguez D, Campbell-Beachler M, Jones T, Stanbouly S, Sridharan V, Wroe A, Nelson GA (2018) Acute effect of low-dose space radiation on mouse retina and retinal endothelial cells. *Radiat Res* 190(1):45–52
- Zhao HW, Zhao J, Hu LN, Liang JN, Shi YY, Nie C, Qiu CY, Nan XS, Li YX, Gao FL, Liu Y, Dong Y, Luo L (2016) Effect of long-term weightlessness on retina and optic nerve in tail-suspension rats. *Int J Ophthalmol* 9(6):825–830
- Tombran-Tink J, Barnstable CJ (2006) Space flight environment induces degeneration in the retina of rat neonates. *Adv Exp Med Biol* 572:417–424

16. Tombran-Tink J, Barnstable CJ (2005) Space shuttle flight environment induces degeneration in the retina of rat neonates. *Gravitational Space Biol Bull* 18(2):97–98
17. Roberts JE, Kukielczak BM, Chignell CF, Sik BH, Hu DN, Principato MA (2006) Simulated microgravity induced damage in human retinal pigment epithelial cells. *Mol Vis* 12:633–638
18. Mader TH, Gibson CR, Caputo M, Hunter N, Taylor G, Charles J, Meehan RT (1993) Intraocular pressure and retinal vascular changes during transient exposure to microgravity. *Am J Ophthalmol* 115(3):347–350
19. Mader TH, Gibson CR, Pass AF, Kramer LA, Lee AG, Fogarty J, Tarver WJ, Dervay JP, Hamilton DR, Sargsyan A, Phillips JL, Tran D, Lipsky W, Choi J, Stern C, Kuyumjian R, Polk JD (2011) Optic disc edema, globe flattening, choroidal folds, and hyperopic shifts observed in astronauts after long-duration space flight. *Ophthalmology* 118(10):2058–2069
20. Mader TH, Gibson CR, Otto CA, Sargsyan AE, Miller NR, Subramanian PS, Hart SF, Lipsky W, Patel NB, Lee AG (2017) Persistent Asymmetric Optic Disc Swelling After Long-Duration Space Flight: Implications for Pathogenesis. *J Neuro-Ophthalmol* 37(2):133–139
21. Zhang LF, Hargens AR (2018) Spaceflight-induced intracranial hypertension and visual impairment: pathophysiology and countermeasures. *Physiol Rev* 98(1):59–87
22. Lee AG, Mader TH, Gibson CR, Tarver W (2017) Space flight-associated neuro-ocular syndrome. *JAMA Ophthalmol* 135(9):992–994
23. Lee AG, Mader TH, Gibson CR, Tarver W, Rabiei P, Riascos RF, Galdamez LA, Brunstetter T (2020) Spaceflight associated neuro-ocular syndrome (SANS) and the neuro-ophthalmologic effects of microgravity: a review and an update. *NPJ Microgravity* 6:7
24. Tymko MM, Boulet LM, Donnelly J (2017) Intracranial pressure in outer space: preparing for the mission to Mars. *J Physiol* 595(14):4587–4588
25. Alwood JS, Ronca AE, Mains RC, Shelhamer MJ, Smith JD, Goodwin TJ (2017) From the bench to exploration medicine: NASA life sciences translational research for human exploration and habitation missions. *NPJ Microgravity* 3:5
26. Lulli M, Cialdai F, Vignali L, Monici M, Luzzi S, Cicconi A, Cacchione S, Magi A, Di Gesualdo F, Balsamo M, Vukich M, Neri G, Donati A, Capaccioli S (2019) The coenzyme Q10 (CoQ10) as countermeasure for retinal damage onboard the international space station: the CORM Project | SpringerLink. *Microgravity Sci Technol* 30(6):925–931
27. Lulli M, Witort E, Papucci L, Torre E, Schiavone N, Dal Monte M, Capaccioli S (2012) Coenzyme Q10 protects retinal cells from apoptosis induced by radiation in vitro and in vivo. *J Radiat Res* 53(5):695–703
28. Lulli M, Witort E, Papucci L, Torre E, Schipani C, Bergamini C, Dal Monte M, Capaccioli S (2012) Coenzyme Q10 instilled as eye drops on the cornea reaches the retina and protects retinal layers from apoptosis in a mouse model of kainate-induced retinal damage. *Invest Ophthalmol Vis Sci* 53(13):8295–8302
29. Papucci L, Schiavone N, Witort E, Donnini M, Lapucci A, Tempestini A, Formigli L, Zecchi-Orlandini S, Orlandini G, Carella G, Brancato R, Capaccioli S (2003) Coenzyme q10 prevents apoptosis by inhibiting mitochondrial depolarization independently of its free radical scavenging property. *J Biol Chem* 278(30):28220–28228
30. Dobin A, Davis CA, Schlesinger F, Drenkow J, Zaleski C, Jha S, Batut P, Chaisson M, Gingeras T (2013) STAR: ultrafast universal RNA-seq aligner. *Bioinformatics (Oxford, England)* 29 (1).
31. Liao Y, Smyth G, Shi K (2014) featureCounts: an efficient general purpose program for assigning sequence reads to genomic features. *Bioinformatics (Oxford, England)* 30 (7).
32. Love M, Huber W, Anders I (2014) Moderated estimation of fold change and dispersion for RNA-seq data with DESeq2. *Genome biology* 15 (12).
33. Ashan S, Drăghici S (2017) Identifying Significantly Impacted Pathways and Putative Mechanisms With iPathwayGuide. *Current protocols in bioinformatics* 57.
34. Corydon TJ, Mann V, Slumstrup L, Kopp S, Sahana J, Askou AL, Magnusson NE, Echegoyen D, Bek T, Sundaresan A, Riwaldt S, Bauer J, Infanger M, Grimm D (2016) Reduced Expression of Cytoskeletal and Extracellular Matrix Genes in Human Adult Retinal Pigment Epithelium Cells Exposed to Simulated Microgravity. *Cellular physiology and biochemistry : international journal of experimental cellular physiology, biochemistry, and pharmacology* 40 (1–2).
35. Krüger M, Pietsch J, Bauer J, Kopp S, Carvalho DTO, Baatout S, Moreels M, Melnik D, Wehland M, Egli M, Jayashree S, Koberø SD, Corydon TJ, Nebuloni S, Gass S, Evert M, Infanger M, Grimm D (2019) Growth of Endothelial Cells in Space and in Simulated Microgravity - a Comparison on the Secretory Level. *Cellular physiology and biochemistry : international journal of experimental cellular physiology, biochemistry, and pharmacology* 52 (5).
36. Wuest SL, Richard S, Kopp S, Grimm D, Egli M (2015) Simulated microgravity: critical review on the use of random positioning machines for mammalian cell culture *BioMed research international* 2015.
37. Moreno-Villanueva M, Wong M, Lu T, Zhang Y, Wu H (2017) Interplay of space radiation and microgravity in DNA damage and DNA damage response. *NPJ microgravity* 3.
38. Larrayoz IM, Rey-Funes M, Contartese DS, Rolón F, Sarotto A, Dorfman VB, Loidl CF, Martínez A (2016) Cold Shock Proteins Are Expressed in the Retina Following Exposure to Low Temperatures. *PloS one* 11 (8).
39. Rey-Funes M, Larrayoz IM, Contartese DS, Soliño M, Sarotto A, Bustelo M, Bruno M, Dorfman VB, Loidl CF, Martínez A (2017) Hypothermia Prevents Retinal Damage Generated by Optic Nerve Trauma in the Rat. *Scientific reports* 7 (1).
40. Lewis ML, Reynolds JL, Cubano LA, Hatton JP, Lawless BD, Piepmeier EH (1998) Spaceflight alters microtubules and increases apoptosis in human lymphocytes (Jurkat). *FASEB J* 12 (11).
41. Locatelli L, Cazzaniga A, De Palma C, Castiglioni S, Maier J (2020) Mitophagy contributes to endothelial adaptation to simulated microgravity. *FASEB J* 34 (1).
42. Maier JA, Cialdai F, Monici M, Morbidelli L (2015) The impact of microgravity and hypergravity on endothelial cells. *BioMed Res Int* 2015.
43. Prasad B, Grimm D, Strauch SM, Erzinger GS, Corydon TJ, Lebert M, Magnusson NE, Infanger M, Richter P, Krüger M (2020) Influence of microgravity on apoptosis in cells, tissues, and other systems in vivo and in vitro. *Int J Mol Sci* 21 (24).
44. Schatten H, Lewis ML, Chakrabarti A (2001) Spaceflight and clinorotation cause cytoskeleton and mitochondria changes and increases in apoptosis in cultured cells. *Acta Astronautica* 49 (3–10).
45. Carlsson SI, Bertilaccio MT, Ballabio E, Maier J (2003) Endothelial stress by gravitational unloading: effects on cell growth and cytoskeletal organization. *Biochimica et Biophysica Acta* 1642 (3).
46. Monici M, Fusi F, Paglierani M, Marziliano N, Cogoli A, Pratesi R, Bernabei PA (2006) Modeled gravitational unloading triggers differentiation and apoptosis in preosteoclastic cells. *J Cell Biochem* 98 (1).
47. Kopp S, Slumstrup L, Corydon TJ, Sahana J, Aleshcheva G, Islam T, Magnusson NE, Wehland M, Bauer J, Infanger M, Grimm D (2016) Identifications of novel mechanisms in breast



- cancer cells involving duct-like multicellular spheroid formation after exposure to the Random Positioning Machine. *Sci Rep* 6.
48. Aleshcheva G, Sahana J, Ma X, Hauslage J, Hemmersbach R, Egli M, Infanger M, Bauer J, Grimm D (2013) Changes in morphology, gene expression and protein content in chondrocytes cultured on a random positioning machine. *PLoS One* 8 (11).
  49. Grimm D, Bauer J, Kossmehl P, Shakibaei M, Schöberger J, Pickenhahn H, Schulze-Tanzil G, Vetter R, Eilles C, Paul M, Cogoli A (2002) Simulated microgravity alters differentiation and increases apoptosis in human follicular thyroid carcinoma cells. *FASEB J* 16 (6).
  50. Morrow CS, Moore DL (2020) Vimentin's side gig: Regulating cellular proteostasis in mammalian systems. *Cytoskeleton (Hoboken, NJ)* 77 (11).
  51. Hu J, Li Y, Hao Y, Zheng T, Gupta SK, Parada GA, Wu H, Lin S, Wang S, Zhao X, Goldman RD, Cai S, Guo M (2019) High stretchability, strength, and toughness of living cells enabled by hyperelastic vimentin intermediate filaments. *Proceedings of the National Academy of Sciences of the United States of America* 116 (35).
  52. Kopito RR (2000) Aggresomes, inclusion bodies and protein aggregation. *Trends Cell Biol* 10 (12).
  53. Koksai AR, Verne GN, Zhou Q (2021) Endoplasmic reticulum stress in biological processing and disease. *J Investigative Med* 69 (2).
  54. Li CF, Pan YK, Gao Y, Shi F, Wang YC, Sun XQ (2019) Autophagy protects HUVECs against ER stress-mediated apoptosis under simulated microgravity. *Apoptosis* 24 (9–10).
  55. Jiang M, Wang H, Liu Z, Lin L, Wang L, Xie M, Li D, Zhang J, Zhang R (2020) Endoplasmic reticulum stress-dependent activation of iNOS/NO-NF- $\kappa$ B signaling and NLRP3 inflammasome contributes to endothelial inflammation and apoptosis associated with microgravity. *FASEB J* 34 (8).
  56. Zhang R, Jiang M, Zhang J, Qiu Y, Li D, Li S, Liu J, Liu C, Fang Z, Cao F (2020) Regulation of the cerebrovascular smooth muscle cell phenotype by mitochondrial oxidative injury and endoplasmic reticulum stress in simulated microgravity rats via the PERK-eIF2 $\alpha$ -ATF4-CHOP pathway. *Biochimica et Biophysica Acta Molecular Basis of Disease* 1866 (8).
  57. Cazzaniga A, Locatelli L, Castiglioni S, Maier JAM (2019) The dynamic adaptation of primary human endothelial cells to simulated microgravity. *FASEB J* 33 (5).
  58. Roca-Portoles A, Tait SWG (2021) Mitochondrial quality control: from molecule to organelle. *Cel Mol Life Sci* 78 (8).
  59. Gertz ML, Chin CR, Tomoiaga D, MacKay M, Chang C, Butler D, Afshinnekoo E, Bezdian D, Schmidt MA, Mozsary C, Melnick A, Garrett-Bakelman F, Crucian B, Lee SMC, Zwart SR, Smith SM, Meydan C, Mason CE (2020) Multi-omic, single-cell, and biochemical profiles of astronauts guide pharmacological strategies for returning to gravity. *Cell Rep* 33 (10).
  60. Nezhich CL, Wang C, Fogel AI, Youle RJ (2015) Mit/TFE transcription factors are activated during mitophagy downstream of Parkin and Atg5. *J Cell Biol* 210 (3).
  61. Ma X, Li H, Chen Y, Yang J, Chen H, Arnheiter H, Hou L (2019) The transcription factor MITF in RPE function and dysfunction. *Progress Retinal Eye Res* 73.
  62. Han S, Chen J, Hua J, Hu X, Jian S, Zheng G, Wang J, Li H, Yang J, Hejtmanek JF, Qu J, Ma X, Hou L (2020) MITF protects against oxidative damage-induced retinal degeneration by regulating the NRF2 pathway in the retinal pigment epithelium. *Redox Biol* 34.
  63. Beheshti A, Ray S, Fogle H, Berrios D, Costes SV (2018) A microRNA signature and TGF-beta1 response were identified as the key master regulators for spaceflight response. *PLoS One* 13 (7):e0199621.
  64. Pluquet O, Hainaut P (2001) Genotoxic and non-genotoxic pathways of p53 induction. *Cancer Lett* 174 (1).
  65. Shi L, Tian H, Wang P, Li L, Zhang Z, Zhang J, Zhao Y (2020) Spaceflight and simulated microgravity suppresses macrophage development via altered RAS/ERK/NF $\kappa$ B and metabolic pathways. *Cell Mol Immunol*.
  66. Dietz C, Infanger M, Romswinkel A, Strube F, Kraus A (2019) Apoptosis Induction and alteration of cell adherence in human lung cancer cells under simulated microgravity. *Int J Mol Sci* 20 (14).
  67. Fukazawa T, Tanimoto K, Shrestha L, Imura T, Takahashi S, Sueda T, Hirohashi N, Hiyama E, Yuge L (2019) Simulated microgravity enhances CDDP-induced apoptosis signal via p53-independent mechanisms in cancer cells. *PLoS One* 14 (7).
  68. Kumari R, Jat P (2021) Mechanisms of cellular senescence: cell cycle arrest and senescence associated secretory phenotype. *Front Cell Dev Biol* 9.
  69. Massagué J (2012) TGF $\beta$  signalling in context. *Nat Rev Mol Cell Biol* 13 (10).
  70. Zhou M, Geathers JS, Grillo SL, Weber SR, Wang W, Zhao Y, Sundstrom JM (2020) Role of epithelial-mesenchymal transition in retinal pigment epithelium dysfunction. *Front Cell Dev Biol* 8.
  71. Ranieri D, Proietti S, Dinicola S, Masiello MG, Rosato B, Ricci G, Cucina A, Catizone A, Bizzarri M, Torrisi MR (2017) Simulated microgravity triggers epithelial mesenchymal transition in human keratinocytes. *Sci Rep* 7 (1).
  72. Chen Z, Shao Y, Li X (2015) The roles of signaling pathways in epithelial-to-mesenchymal transition of PVR. *Mol Vis* 21.
  73. Chen Y, Wu B, He JF, Chen J, Kang ZW, Liu D, Luo J, Fang K, Leng X, Tian H, Xu J, Jin C, Zhang J, Wang J, Zhang J, Ou Q, Lu L, Gao F, Xu GT (2021) Effectively intervening epithelial-mesenchymal transition of retinal pigment epithelial cells with a combination of ROCK and TGF- $\beta$  signaling inhibitors. *Investigative Ophthalmol Vis Sc* 62 (4).
  74. Du Y, Chen Q, Huang L, Wang S, Yin X, Zhou L, Ye Z, Ren X, Cai Y, Ding X, Ouyang H, Li X, Ju H (2018) VEGFR2 and VEGF-C Suppresses the epithelial-mesenchymal transition Via YAP in Retinal Pigment Epithelial Cells. *Curr Mol Med* 18 (5).
  75. Wilson SE (2021) TGF beta -1, -2 and -3 in the modulation of fibrosis in the cornea and other organs. *Experimental eye research* 207.
  76. Moon S, Lee S, Caesar JA, Pruchenko S, Leask A, Knowles JA, Sinon J, Chaqour B (2020) A CTGF-YAP Regulatory Pathway Essential for Angiogenesis and Barrierogenesis in the Retina. *iScience* 23 (6).
  77. Lau LF (2016) Cell surface receptors for CCN proteins. *J Cell Commun Signal* 10 (2).
  78. Hinton DR, He S, Jin ML, Barron E, Ryan SJ (2002) Novel growth factors involved in the pathogenesis of proliferative vitreoretinopathy. *Eye (London, England)* 16 (4).
  79. Di Gesualdo F, Capaccioli S, Lulli M (2014) A pathophysiological view of the long non-coding RNA world. *Oncotarget* 5(22):10976–10996
  80. Wang Y, Wang K, Zhang L, Tan Y, Hu Z, Dang L, Zhou H, Li G, Wang H, Zhang S, Shi F, Cao X, Zhang G (2020) Targeted overexpression of the long noncoding RNA ODSM can regulate osteoblast function in vitro and in vivo. *Cell death & disease* 11 (2).
  81. Fu H, Su F, Zhu J, Zheng X, Ge C (2020) Effect of simulated microgravity and ionizing radiation on expression profiles of miRNA, lncRNA, and mRNA in human lymphoblastoid cells. *Life sciences in space research* 24.
  82. Thiel CS, Hauschild S, Hüge A, Tauber S, Lauber BA, Polzer J, Paulsen K, Lier H, Engelmann F, Schmitz B, Schütte A, Layer

- LE, Ullrich O (2017) Dynamic gene expression response to altered gravity in human T cells. *Scientific reports* 7 (1).
83. Luo R, Li L, Hu YX, Xiao F (2021) LncRNA H19 inhibits high glucose-induced inflammatory responses of human retinal epithelial cells by targeting miR-19b to increase SIRT1 expression. *Kaohsiung J Med Sci* 37 (2).
  84. Thomas AA, Biswas S, Feng B, Chen S, Gonder J, Chakrabarti S (2019) lncRNA H19 prevents endothelial-mesenchymal transition in diabetic retinopathy. *Diabetologia* 62 (3).
  85. Liang J, Liao J, Liu T, Wang Y, Wen J, Cai N, Huang Z, Xu W, Li G, Ding Z, Zhang B (2020) Comprehensive analysis of TGF- $\beta$ -induced mRNAs and ncRNAs in hepatocellular carcinoma. *Aging* 12 (19).
  86. Zhang LC, Wei ZB, Tang SF (2020) Knockdown of the long non-coding RNA LUCAT1 inhibits high-glucose-induced epithelial-mesenchymal transition through the miR-199a-5p-ZEB1 axis in human renal tubular epithelial cells. *BioMed Res Int* 2020.
  87. Bartel DP (2004) MicroRNAs: genomics, biogenesis, mechanism, and function. *Cell* 116 (2).
  88. Witort E, Lulli M, Carloni V, Capaccioli S (2013) Anticancer activity of an antisense oligonucleotide targeting TRADD combined with proteasome inhibitors in chemoresistant hepatocellular carcinoma cells. *J Chemotherapy (Florence, Italy)* 25 (5).
  89. Malkani S, Chin CR, Cekanaviciute E, Mortreux M, Okinula H, Tarbier M, Schreurs AS, Shirazi-Fard Y, Tahimic CGT, Rodriguez DN, Sexton BS, Butler D, Verma A, Bezdán D, Durmaz C, MacKay M, Melnick A, Meydan C, Li S, Garrett-Bakelman F, Fromm B, Afshinnekoo E, Langhorst BW, Dimalanta ET, Cheng-Campbell M, Blaber E, Schisler JC, Vanderburg C, Friedländer MR, McDonald JT, Costes SV, Rutkove S, Grabham P, Mason CE, Beheshti A (2020) Circulating miRNA Spaceflight Signature Reveals Targets for Countermeasure Development. *Cell Rep* 33 (10).
  90. Kasiviswanathan D, Chinnasamy Perumal R, Bhuvaneshwari S, Kumar P, Sundaresan L, Philip M, Puthenpurackal Krishnankutty S, Chatterjee S (2020) Interactome of miRNAs and transcriptome of human umbilical cord endothelial cells exposed to short-term simulated microgravity. *NPJ Microgravity* 6.
  91. Qin W, Liu L, Wang Y, Wang Z, Yang A, Wang T (2019) Mir-494 inhibits osteoblast differentiation by regulating BMP signaling in simulated microgravity. *Endocrine* 65 (2).
  92. Gong L, Wu X, Li X, Ni X, Gu W, Wang X, Ji H, Hu L, Zhu L (2020) S1PR3 deficiency alleviates radiation-induced pulmonary fibrosis through the regulation of epithelial-mesenchymal transition by targeting miR-495-3p. *J Cell Physiol* 235 (3).
  93. Ma Y, Duan J, Hao X (2020) Down-regulated HDAC3 elevates microRNA-495-3p to restrain epithelial-mesenchymal transition and oncogenicity of melanoma cells via reducing TRAF5. *J Cell Mol Med* 24 (22).
  94. Jiang H, Huang G, Zhao N, Zhang T, Jiang M, He Y, Zhou X, Jiang X (2018) Long non-coding RNA TPT1-AS1 promotes cell growth and metastasis in cervical cancer via acting AS a sponge for miR-324-5p. *J Exp Clin Cancer Res* 37 (1).
  95. Zhang Q, Liu H, Zhang J, Shan L, Yibureyimu B, Nurlan A, Aexiding P, Luo Q (2020) MiR-142-5p suppresses lung cancer cell metastasis by targeting Yin Yang 1 to regulate epithelial-mesenchymal transition. *Cell Reprogramming* 22 (6).
  96. Qu J, Kaufman Y, Washington I (2009) Coenzyme Q10 in the human retina. *Investigative Ophthalmol Vis Sci* 50 (4).
  97. Semenza GL (2000) HIF-1: mediator of physiological and pathophysiological responses to hypoxia. *J Appl Physiol (Bethesda, Md: 1985)* 88 (4).
  98. Li WY, Zhou HZ, Chen Y, Cai XF, Tang H, Ren JH, Wai Wong VK, Kwan Law BY, Cheng ST, Yu HB, Cai HY, Chen WX, Tang N, Zhang WL, Tao NN, Yang QX, Ren F, He L, Jiang H, Huang AL, Chen J (2019) NAD(P)H: quinone oxidoreductase 1 overexpression in hepatocellular carcinoma potentiates apoptosis evasion through regulating stabilization of X-linked inhibitor of apoptosis protein. *Cancer Lett* 451:156–167
  99. Vogel J, Thiel CS, Tauber S, Stockmann C, Gassmann M, Ullrich O (2019) Expression of Hypoxia-Inducible Factor 1 $\alpha$  (HIF-1 $\alpha$ ) and Genes of Related Pathways in Altered Gravity. *Int J Mol Sci* 20 (2).
  100. Dixon SJ, Lemberg KM, Lamprecht MR, Skouta R, Zaitsev EM, Gleason CE, Patel DN, Bauer AJ, Cantley AM, Yang WS, Morrison B, Stockwell BR (2012) Ferroptosis: an iron-dependent form of nonapoptotic cell death. *Cell* 149 (5).
  101. Alvarez SW, Sviderskiy VO, Terzi EM, Papagiannakopoulos T, Moreira AL, Adams S, Sabatini DM, Birsoy K, Possemato R (2017) NFS1 undergoes positive selection in lung tumours and protects cells from ferroptosis. *Nature* 551 (7682).
  102. Dixon SJ, Patel DN, Welsch M, Skouta R, Lee ED, Hayano M, Thomas AG, Gleason CE, Tatonetti NP, Slusher BS, Stockwell BR (2014) Pharmacological inhibition of cystine-glutamate exchange induces endoplasmic reticulum stress and ferroptosis. *eLife* 3.
  103. Santoro M (2020) The Antioxidant Role of Non-mitochondrial CoQ10: Mystery Solved! *Cell metabolism* 31 (1).
  104. Yang S, Zhou J, Li D (2021) Functions and diseases of the retinal pigment epithelium. *Front Pharmacol* 12.
  105. Zarbin M (2016) Cell-Based Therapy for degenerative retinal disease. *Trends Mol Med* 22 (2).
  106. Xia T, Rizzolo LJ (2017) Effects of diabetic retinopathy on the barrier functions of the retinal pigment epithelium. *Vis Res* 139.
  107. Overbey EG, da Silveira WA, Stanbouly S, Nishiyama NC, Roque-Torres GD, Pecaut MJ, Zawieja DC, Wang C, Willey JS, Delp MD, Hardiman G, Mao XW (2019) Spaceflight influences gene expression, photoreceptor integrity, and oxidative stress-related damage in the murine retina. *Scientific reports* 9 (1).
  108. Patel ZS, Brunstetter TJ, Tarver WJ, Whitmire AM, Zwart SR, Smith SM, Huff JL (2020) Red risks for a journey to the red planet: The highest priority human health risks for a mission to Mars. *NPJ Microgravity* 6 (1).
  109. Iosim S, MacKay M, Westover C, Mason CE (2019) Translating current biomedical therapies for long duration, deep space missions. *Precision clinical medicine* 2 (4).
  110. Rea G, Cristofaro F, Pani G, Pascucci B, Ghuge SA, Corsetto PA, Imbriani M, Visai L, Rizzo AM (2016) Microgravity-driven remodeling of the proteome reveals insights into molecular mechanisms and signal networks involved in response to the space flight environment. *J Proteomics* 137.

**Publisher's Note** Springer Nature remains neutral with regard to jurisdictional claims in published maps and institutional affiliations.